COMMUNICATIONS IN COMPUTATIONAL PHYSICS
Vol. **6**, No. 1, pp. 109-130

Commun. Comput. Phys.
July 2009

Wavelet Galerkin Methods for Aerosol Dynamic Equations in Atmospheric Environment

Dong Liang[1,*], Qiang Guo[1] and Sunling Gong[2]

[1] *Department of Mathematics and Statistics, York University, 4700 Keele Street, Toronto, Ontario, M3J 1P3, Canada.*
[2] *Air Quality Research Division, S & T Branch, Environment Canada, 4905 Dufferin Street, Toronto, Ontario, M3H 5T4, Canada.*

Received 14 January 2008; Accepted (in revised version) 10 September 2008

Available online 18 November 2008

Abstract. Aerosol modelling is very important to study and simulate the behavior of aerosol dynamics in atmospheric environment. In this paper, we consider the general nonlinear aerosol dynamic equations which describe the evolution of the aerosol distribution. Continuous time and discrete time wavelet Galerkin methods are proposed for solving this problem. By using the Schauder's fixed point theorem and the variational technique, the global existence and uniqueness of solution of continuous time wavelet numerical methods are established for the nonlinear aerosol dynamics with sufficiently smooth initial conditions. Optimal error estimates are obtained for both continuous and discrete time wavelet Galerkin schemes. Numerical examples are given to show the efficiency of the wavelet technique.

AMS subject classifications: 52B10, 65D18, 68U05, 68U07

Key words: Aerosol dynamics, wavelet Galerkin methods, semi-discrete, fully-discrete, existence, error estimate.

1 Introduction

The distribution of aerosol particles in atmospheric environment has been recognized to be of significance due to their effects on climate change and human health. Aerosol modeling has been playing an important role in studying and simulating the behavior of aerosol dynamics in atmosphere. The aerosol dynamic equations in terms of the aerosol size distribution function describe different processes evolved in the lifetime of aerosols, which include condensation, nucleation, coagulation, and deposition. The equations are

*Corresponding author. *Email addresses:* dliang@mathstat.yorku.ca (D. Liang), ppguo@mathstat.yorku.ca (Q. Guo), sunling.gong@ec.gc.ca (S. Gong)

nonlinear differential and integral equations. Some numerical methods have been studied to solve the equations such as sectional method [21], moment method [5, 32], modal method [2, 36], finite element method [31], and stochastic approach [17], etc. The conventional sectional approach has some limitation such as numerical diffusion and lower accuracy, while the modal approach has the high numerical efficiency but less physical representation of real aerosol distribution and overlap of various models [35]. But, on the other hand, there have been few works on the theoretical analysis of numerical methods to the nonlinear aerosol dynamics which will definitely indicate to develop efficient numerical techniques for the problem.

Wavelet multiresolution analysis was originally applied as a powerful tool for signal and image processing. Wavelets cut up data into different frequency components and then study each component with a resolution matched to its scale. The wavelet technique has great advantage of approximating the signals which contain discontinuities and sharp spikes. Recently, wavelet techniques have been applied to many areas in applied mathematics including developing numerical schemes to solve the integral equations and the partial differential equations (see, e.g., [1, 7, 8, 10, 11, 13–15, 23, 24, 29, 33]). Papers [10, 15, 29] developed efficient multilevel wavelet methods for solving nonlinear integral equations on bounded domains. [7, 13] developed wavelet Galerkin methods for the numerical solution of second-order elliptic equations. Paper [1] considered wavelet Galerkin methods for solving quasilinear hyperbolic conservation equations. [14] studied generalized Petrov-Galerkin schemes with multiscale techniques for solving pseudodifferential equations. [33] studied wavelet methods for parabolic problems combining with a strongly elliptic pseudodifferential operator. Recently, paper [24] applied the wavelet collocation method to compute the population balance equation. However, there is no theoretical analysis provided for the methods to this problem.

Due to the localization properties that wavelets display both in space and frequency, the wavelet multiresolution analysis allows us to obtain an efficient sparse representation of the solution function, especially useful when the solution contains singularities, irregular structure and transient phenomena. Wavelet methods can distinguish smooth and singular regions automatically. This leads to the most important advantage that the wavelets can efficiently and accurately approximate sharp changes of solution functions. On the other aspect, due to different condensation, coagulation and removal mechanisms, the aerosol size distribution is highly uneven distributed, such as multiple lognormal distributions in some regions. Thus, it is very important to efficiently solve the aerosol dynamic equations in size and time where the aerosol distributions vary very sharply in the size direction. This motivates us to develop and analyze wavelet Galerkin methods for solving the aerosol dynamic equations in this paper.

In this paper, we propose and analyze wavelet Galerkin methods for solving the nonlinear aerosol dynamic equations. The aerosol dynamic equations are nonlinear differential and integral equations which contain a nonlinear Volterra type integral term and a nonlinear Fredholm type integral term of the size distribution function. We introduce wavelet Galerkin methods to construct both the semi-discrete scheme and the

fully-discrete scheme for the nonlinear aerosol dynamic equations. Compactly supported wavelets on the bounded domain based on the Daubechies' scaling and wavelet functions are applied in the Galerkin scheme due to several good properties of them. We prove the global existence and uniqueness of the approximate solution for the nonlinear problem of the semi-discrete wavelet Galerkin scheme by the theory of variation methods and the Schauder's fixed point theorem. The error estimates in L^2 norm are obtained for both the semi-discrete and fully discrete wavelet Galerkin schemes. Numerical experiments are given to illustrate the efficiency of the wavelet Galerkin scheme. To the best of our knowledge, our work in the paper is the first theoretical work to numerical wavelet methods of aerosol dynamic equations. Thus, the work has significance in both theoretical analysis and application of the nonlinear equations of aerosol dynamics.

This paper is organized as follows. In Section 2, we describe the nonlinear model of the aerosol dynamics. After introducing the basic properties of wavelet and approximation theory, we propose the semi-discrete and fully discrete wavelet Galerkin schemes for the nonlinear aerosol dynamics in Section 3. Then, in Section 4, we derive error analysis for semi-discrete scheme and further in Section 5, the global existence and uniqueness of the approximation solution are proved. In Section 6, we analyze error estimates for the fully-discrete scheme. Numerical examples are given in Section 7. Finally, we draw some conclusions in Section 8.

2 Aerosol dynamics model

Consider aerosol dynamic equations (see [20, 22, 31])

$$\frac{\partial u(v,t)}{\partial t} = -\frac{\partial (G(v)u(v,t))}{\partial v} + \frac{1}{2}\int_{V_{\min}}^{v-V_{\min}} \beta(v-w,w)u(v-w,t)u(w,t)dw - \int_{V_{\min}}^{V_{\max}} \beta(v,w)u(v,t)u(w,t)dw - R(v)u(v,t), \tag{2.1}$$

$$u(V_{\min},t) = 0, \quad t \in (0,T], \tag{2.2}$$

$$u(v,0) = u_0(v), \quad v \in [V_{\min}, V_{\max}], \tag{2.3}$$

where $t>0$ is the time, v is the aerosol particle volume, $T>0$ is the time period. $u(v,t)$ is the number concentration distribution function of aerosol particles. In practice one assumes that the particle population has a nonzero minimal volume and a finite maximal volume, i.e., the dynamic equation is solved in a finite volume interval $[V_{\min}, V_{\max}]$, where $V_{\min}$ and $V_{\max}$ are chosen as lower and upper limits of the aerosol volume respectively. The first term on the right-hand side of Eq. (2.1) is the condensation process which describes the net rate of change, per unit volume of air, of particles of volume v due to condensation of vapor species onto the particles. The condensation growth rate $G(v)$ is defined as the rate of change of the volume of a particle of volume v. The second term on the right-hand side of Eq. (2.1) is an integral of Volterra type which describes the creation

of particles of volume v by coagulation of smaller particles. The third term is an integral of Fredholm type which models the loss of volume v particles due to coagulation. Coagulation of aerosol particles may occur through a variety of mechanisms such as Brownian motion, turbulent diffusion, etc. The coefficient $\beta(v,w)$ is the coagulation kernel between two particles of volume v and w entering collision.

The forms of the growth rate $G(v)$ and the coagulation kernel $\beta(v,w)$ have close relations with the atmospherical surroundings. The condensation growth rate can be described as: $G(v)=G_\gamma v^\gamma$, $0<\gamma\leq 1$, where G_γ is a positive number involving numerical and physical constants and difference in vapor pressure of the diffusing species in bulk gas [19, 22]. Three cases of growth rate $G(v)$ are widely used in applications, which are linear growth rate, condensation growth in free molecule size regime and in continuum size regime [5, 20, 22]. The coagulation is mostly due to the Brownian activity. The coagulation kernel in the continuum size regime can be written for spherical aerosols of size v and w as (see [17, 20]):

$$\beta(v,w)=\frac{2k_bTe}{3\mu_{air}}\left[2+\left(\frac{v}{w}\right)^{1/3}+\left(\frac{w}{v}\right)^{1/3}\right], \tag{2.4}$$

where $k_b=1.381\times10^{-23}JK^{-1}$ is the Boltzmann's constant, μ_{air} is the dynamic viscosity of air and Te is the temperature. It is noted that the Brownian kernel can be considered in first approximation as a constant (see [20]); indeed for equal size aerosols the coagulation kernel is reduced to $\bar{\beta}=8k_bTe/(3\mu_{air})$, where $\bar{\beta}$ is usually called the Brownian constant. When taking the temperature $Te=298K$ and the dynamic viscosity of air $\mu_{air}=6.552\times10^{-2}kg/mhour$, it is equal to $2.166\times10^{-6}cm^3/hour$ for average atmospheric conditions. On the finite volume interval, the coagulation kernel is bounded, $\beta(x,y)\leq\beta_0$. The removal term, the last term on the right side of Eq. (2.1), denotes particles of volume v lost due to sinks of aerosols. $R(v)$ is the removal rate for a particle of volume v and there exists a positive real number R_0 such that $R(v)\leq R_0$.

In computation, we select a dimensionless finite particle size x scaled into interval $\Omega=[0,1]$ through transformation $x=av+b$, where $a=1/(V_{\max}-V_{\min})$, $b=-V_{\min}/(V_{\max}-V_{\min})$ (see [22, 31]). Then we have the corresponding equation

$$\begin{aligned}\frac{\partial u(x,t)}{\partial t}=&-\frac{\partial[G(x)u(x,t)]}{\partial x}+\int_0^x\beta(x-y,y)u(x-y,t)u(y,t)dy\\&-\frac{1}{a_1}u(x,t)\int_0^1\beta(x,y)u(y,t)dy-R(x)u(x,t),\quad (x,t)\in\Omega\times(0,T],\end{aligned} \tag{2.5}$$

$$u(0,t)=0,\quad t\in(0,T], \tag{2.6}$$

$$u(x,0)=u_0(x),\quad x\in\Omega, \tag{2.7}$$

where $G(x)=aG(v)$ and $\beta(x,y)=\frac{1}{2a}\beta(v,w)$.

The aerosol dynamic equation (2.1) or (2.5) is a nonlinear integral and differential equation which includes the nonlinear Volterra type and Fredholm type integral terms of coagulation and the transport term of condensation. The diameter of aerosol particles can

span orders of magnitude, from a few nanometer to several micrometer. Atmospheric particles are usually classified into different groups corresponding to their sizes. Due to different condensation, coagulation and removal mechanisms evolved with different groups, the aerosol size distribution is highly uneven distributed, such as multiple log-normal distributions in some regions. Thus, the most important problem encountered in the solution of this equation is how to efficiently solve the equation in size and time since the aerosol distribution varies very sharply in the size direction. The wavelet technique is relatively new developed method and is widely used in digital signal processing and image compression. The wavelet expansion can be viewed as a localized analysis with multiresolution structure that automatically cuts up functions into different frequency components, and thus study each component with a resolution to match its scale. This leads to the most important advantage that the wavelets can efficiently and accurately approximate sharp changes of functions. This motivates us to develop and analyze wavelet Galerkin methods for solving the aerosol dynamic equation (2.5) in this paper.

3 Wavelet Galerkin methods

We denote by $L^2(\Omega)$ the usual square integrable functions with inner product $\langle\cdot,\cdot\rangle$ and the associated norm by $\|\cdot\|$ and by $H^s(\Omega)$ the standard Sobolev space with norm $\|\cdot\|_s$. Further we define the space $H_E^1(\Omega)=\{v\in H^1(\Omega):v(0)=0\}$. Let also $\|\cdot\|_\infty$ denote the norm on $L^\infty(\Omega)$. If $(X,\|\cdot\|_X)$ is a Banach space, $L^\infty(0,T;X)$ will be the Banach space of strongly measurable functions $f:[0,T]\longrightarrow X$ such that

$$\|f\|_{L^\infty(0,T;X)}=\sup_{0<t\leq T}\|f(t)\|_X<\infty. \tag{3.1}$$

Remark 3.1. The existence and uniqueness of the solution to aerosol dynamic equation (2.5) refers to [6]. Henceforth, it will be assumed Eq. (2.5) has a unique solution u which belongs to $H_E^1(\Omega)$ for $t\in[0,T]$. Further, the required smoothness of the solution will be made when needed in analysis in Sections 4-6.

Wavelets have emerged in the last decades as a synthesis of ideas from fields as different as electrical engineering, physics and mathematics. Multiresolution analysis (MRA) is one of the most sophisticated ways of generating wavelets in $L^2(\mathbb{R})$ (see, for example, [16,25]), which is defined as a sequence of closed subspaces V_j such that:

$$V_j\subset V_{j+1},\quad j\in\mathbb{Z};\quad \bigcap_{j\in\mathbb{Z}}V_j=\{0\};\quad \overline{\bigcup_{j\in\mathbb{Z}}V_j}=L^2(\mathbb{R}); \tag{3.2}$$

$$f(x)\in V_j\Leftrightarrow f(2x)\in V_{j+1},\quad j\in\mathbb{Z}; \tag{3.3}$$

$$f\in V_0\Leftrightarrow f(\cdot-k)\in V_0,\quad k\in\mathbb{Z}. \tag{3.4}$$

There exists a scaling function ϕ, of which the translation and dilation generate the basis of V_j via

$$V_j=\overline{\text{span}\{\phi_{j,k}\}_{k\in\mathbb{Z}}},$$

with

$$\phi_{j,k}(x)=2^{j/2}\phi(2^j x-k),\quad j,k\in\mathbb{Z}.$$

We denote the orthogonal complement of V_j in V_{j-1} by W_{j-1},

$$V_j=V_{j-1}\oplus W_{j-1}. \tag{3.5}$$

Then each element of V_j can be uniquely written as the sum of an element in V_{j-1} and an element in W_{j-1}, which contains the details needed to pass from an approximation at level $j-1$ to an approximation at level j. A basis function ψ for W_0 is called a wavelet. Similarly, we have

$$W_j=\overline{\text{span}\{\psi_{j,k}\}_{k\in\mathbb{Z}}},$$

where

$$\psi_{j,k}(x)=2^{j/2}\psi(2^j x-k),\quad j,k\in\mathbb{Z}.$$

Daubechies in [16] constructed the most well-known family of wavelets, which include members from highly localized to highly smooth. The family of compactly supported orthonormal wavelets constructed by Daubechies' possesses the advantage of orthogonality, compact support, and exact representation by polynomials of a fixed degree (see, [7]). The support of the Daubechies' scaling function is $[0,2N-1]$, where $N>0$ is an integer. The size of the support increases linearly with the regularity. Moreover, the wavelet function ψ has the support $[1-N,N]$ and has N vanishing moments

$$\int_{-\infty}^{\infty}x^k\psi(x)dx=0,\quad k=0,1,\cdots,N-1. \tag{3.6}$$

All the above concerns bases for $L^2(\mathbb{R})$.

In both theory and application of wavelets, multiresolution analysis and wavelets can be obtained on bounded intervals. While keeping the interior basis functions which have the compact supports in the bounded interval, for several basis functions which straddle the boundary, one needs to reconstruct these several basis functions for satisfying the boundary conditions as well as other properties if needed. Based on the shifted Daubechies' scaling and wavelet functions verifying *supp* ϕ = *supp* $\psi=[0,2N-1]$, a sequence of subspaces $V_j(\Omega)$ and $W_j(\Omega)$ on the interval $\Omega=[0,1]$ can be constructed (See, for example [12,37], etc). Suppose that a level integer $J_0>0$ satisfies $2^{J_0}>2N$. The interior basis functions are $\{\phi_{j,k},\ j\geq J_0,\ 0\leq k\leq 2^j-2N+1\}$ and $\{\psi_{j,k},\ j\geq J_0,\ 0\leq k\leq 2^j-2N+1\}$, which are simply scaling and wavelet functions defined above and satisfy $\text{supp}(\phi_{j,k})=[k/2^j,(2N-1+k)/2^j]\subset[0,1]$ and $\text{supp}(\psi_{j,k})=[k/2^j,(2N-1+k)/2^j]\subset[0,1]$. For the N scaling functions with the support intersecting with the left boundary, we need replace them by N boundary scaling functions $\{\tilde{\phi}_j^n\}$ at each level $j\geq J_0$. Let $\{\tilde{\phi}^n\}$, $n=0,\cdots,N-1$,

be constructed by the linear combinations of $\{\phi_k\}, 2-2N \le k \le 0$ and the Gram-Schmidt procedure as well as satisfying $\tilde{\phi}^n(0)=0$. Denote $\tilde{\phi}^n_j(x)=2^{j/2}\tilde{\phi}^n(2^j x)$ for $j \ge J_0$. Then the N boundary scaling functions $\{\tilde{\phi}^n_j\}, n=0,\cdots,N-1$, are independent and orthogonal both to each other and to all the interior functions $\{\phi_{j,k},\ j \ge J_0,\ 0 \le k \le 2^j-2N+1\}$, and $\tilde{\phi}^n_j(0)=0, n=0,\cdots,N-1$. Similarly, we can construct right edge scaling functions $\{\bar{\phi}^n_j\}, n=0,\cdots,N-1$, satisfying the orthogonality. Then the subspace $V_j(\Omega)$ is defined by setting

$$V_j(\Omega)=\text{span}\{\phi_{j,k}, k=0,\cdots,2^j-1,\ \tilde{\phi}^n_j, n=0,\cdots,N-1,\ \bar{\phi}^n_j, n=0,\cdots,N-1\} \tag{3.7}$$

for $j \ge J_0$. It satisfies $V_j(\Omega) \subset H^1_E(\Omega)$.

With $\{\tilde{\phi}^n\}, n=0,\cdots,N-1$, we can define $\{\tilde{\psi}^n\}, n=0,\cdots,N-1$ as the linear combination of $\{\tilde{\phi}^n_1\}_{0\le n\le N-1}$ and $\{\phi_{1,k}\}_{1\le k\le 2N-1}$

$$\tilde{\psi}^n=\tilde{\phi}^n_1-\sum_{m=0}^{N-1}\langle\tilde{\phi}^n_1,\tilde{\phi}^m\rangle\tilde{\phi}^m. \tag{3.8}$$

and $\tilde{\psi}^n_j(x)=2^{j/2}\tilde{\psi}^n(2^j x)$ for $j \ge J_0$. As usual, we can define $W_j(\Omega)$ by

$$W_j(\Omega)=\text{span}\{\psi_{j,k}, k=0,\cdots,2^j-1,\ \tilde{\psi}^n_j, n=0,\cdots,N-1,\ \bar{\psi}^n_j, n=0,\cdots,N-1\} \tag{3.9}$$

for $j \ge J_0$. We have that

$$V_j(\Omega)=V_{j-1}(\Omega)\oplus W_{j-1}(\Omega)$$

for $j-1 \ge J_0$.

We refer the detailed construction process to [12, 37]. Other methods to construct scaling and wavelet basis functions on $[0,1]$ based on Daubechies' functions can be found in [3, 26]. Moreover, $V_j(\Omega)$ satisfies the following properties (see [12, 37]):

(i) Approximation property: Let $j \ge J_0$ and for any $u \in H^s(\Omega)\bigcup H^1_E(\Omega)$, there exists a constant C_1 independent of j and u such that

$$\inf_{w\in V_j(\Omega)}\|u-w\|_i \le C_1 2^{-(s-i)j}\|u\|_s, \quad i=0,1,\ 0\le s\le N. \tag{3.10}$$

(ii) Inverse property: For $w \in V_j(\Omega)$, there is a constant C_2 independent of j and w such that

$$\|w\|_1 \le C_2 2^j \|w\|. \tag{3.11}$$

For convenience, we define the following linear operator $\mathcal{L}_1 u$ and nonlinear operators $\mathcal{L}_2(u)$ and $\mathcal{L}_3(u)$:

$$\mathcal{L}_1 u = -\frac{\partial(G(x)u(x,t))}{\partial x}, \tag{3.12}$$

$$\mathcal{L}_2(u) = \frac{1}{2}\int_0^x \beta(x-y,y)u(x-y,t)u(y,t)dy, \tag{3.13}$$

$$\mathcal{L}_3(u) = \int_0^1 \beta(x,y)u(x,t)u(y,t)dy. \tag{3.14}$$

Then, problem (2.5)-(2.7) has the following weak formulation: Find $u:\ [0,T] \longrightarrow H_E^1(\Omega)$, such that

$$\langle u_t,v\rangle = \langle \mathcal{L}_1 u,v\rangle - \langle R(x)u,v\rangle + \langle \mathcal{L}_2(u),v\rangle - \langle \mathcal{L}_3(u),v\rangle, \quad v\in H_E^1(\Omega), \tag{3.15}$$

$$\langle u(\cdot,0),v\rangle = \langle u_0,v\rangle, \quad v\in H_E^1(\Omega). \tag{3.16}$$

Thus, the semi-discrete wavelet Galerkin approximation to the solution of (3.15)-(3.16) in the finite-dimensional wavelet subspace $V_j(\Omega)$ is defined as follows: Find $U(t)\in V_j(\Omega)$ such that for $t\in[0,T]$,

$$\langle U_t,v\rangle - \langle \mathcal{L}_1 U,v\rangle + \langle R(x)U,v\rangle = \langle \mathcal{L}_2(U),v\rangle - \langle \mathcal{L}_3(U),v\rangle, \ v\in V_j(\Omega), \tag{3.17}$$

with $U(0)=P_j u_0$, where P_j is an appropriate projection onto $V_j(\Omega)$.

Further, let $\Delta t>0$ be the time step size, $L=T/\Delta t\in Z$, and $t^l=l\Delta t$, $l=0,1,\cdots,L$. Denote $U^l=U(x,t^l)$. Finally, we can define the fully discrete wavelet Galerkin scheme for the problem as: For $l\geq 0$, find $U^{l+1}\in V_j(\Omega)$ such that

$$\begin{aligned}&\left\langle \frac{U^{l+1}-U^l}{\Delta t},v\right\rangle - \langle \mathcal{L}_1 U^{l+1},v\rangle + \left\langle R(x)U^{l+1},v\right\rangle \\ =&\left\langle \mathcal{L}_2(U^l),v\right\rangle - \left\langle \mathcal{L}_3(U^l),v\right\rangle, \quad v\in V_j(\Omega),\end{aligned} \tag{3.18}$$

with $U^0=P_j u_0$.

Remark 3.2. We have used Daubechies' wavelets as the solution bases for the reason that it offers several properties of orthogonality, compact support, exact representation of polynomials to a certain degree, and ability to represent functions at different levels of resolution. In scheme (3.18), the coefficient matrix for the first term on the left-hand side is a diagonal matrix. The coefficient matrices of the second term and third term on the left-hand side are band-diagonal matrices due to the compactness of the Daubechies' wavelets. The terms on the right-hand side are approximated by the previous level values, which go into the right-hand side vector of the linear system of equations.

On the other hand, Daubechies' wavelets have the capability of representing solutions at different levels of resolution, which makes them particularly useful in building

the relation of higher resolution level and lower resolution level of wavelets. Recursive application of the dyadic coupling relation between two consecutive resolution levels will give the fast "pyramid" scheme for computing the expansion coefficients of the unknown function. The use of this relation of higher resolution level and lower resolution level of wavelets can lead to further construct the fast numerical algorithms for the elements of the matrices by the pyramid scheme (see [4] for more details). Meanwhile, since Daubechies' wavelets are orthonormal and have compact support, one can get the relations between the decay of the coefficients and different resolution levels. The property of the fast decay between different scales can lead to compress the coefficient matrices [34].

Remark 3.3. Another advantage of wavelet methods is to design the adaptive algorithm. More recently, adaptive wavelet methods have been recognized to be important adaptive techniques in the applications to solutions of PDEs (see, [13, 15, 18, 30], etc). For many real problems, solutions often exhibit localized singular features such as sharp peaks. Uniform basis functions in space is not a practical option since high resolution is only needed in small regions. Adaptive methods bring forward significant improvements in accuracy and computational efficiency. The localization property of the wavelets both in space and in frequency makes the adaptivity efficiently. The multi-resolution of wavelets is a simple and efficient way for designing adaptive algorithms. The resolution level of the solution, which is closely related to the grid size and the length of the wavelet series, can be chosen adaptively according to the smoothness of the function at different locations. In smooth regions few wavelet coefficients are needed and, in singular regions, large variations in the function require more wavelet coefficients. One can optimize the computational effort by choosing adaptively grids and bases corresponding to the local regularity of the solution. This result leads to efficient adaptive methods for solving PDEs. We will further study and analyze the adaptive wavelet methods for solving the aerosol dynamic equation in the next paper.

Remark 3.4. Another important area is the study of wavelet methods for solving operator equations (integral equations). In this area, many papers have obtained important results ([9, 10, 15, 27–29], etc). For solving this kind bounded domain problems, [27, 28] constructed orthonormal multiwavelets bases on bounded domain. In [27], wavelets were constructed by using the matrix refinement equation and the basic operations of translations and scales, which are not smooth but of small support and can be made to have vanishing moments. [28] constructed biorthogonal multiwavelets through a recursive formula from one level to another. In [9] interpolating wavelets were constructed on invariant sets. These multiwavelets on bounded domains have been studied for efficiently solving the operator equations (integral equations) (see [10, 15, 29], etc). The multiscale representation of integral operators based on these wavelets lead to linear systems with sparse coefficients matrices whose condition numbers are bounded. These sparse representations form the base of fast numerical algorithms for solving such integral equations. On the other hand, in the standard Galerkin formulation of partial differential equations, one needs the multiwavelet function spaces $V_j(\Omega) \subset H_E^1(\Omega)$ or $H_0^1(\Omega)$. Therefore, when

the multiwavelets above are discontinuous on the domain Ω, these discontinuous orthogonal multiwavelets could be applied to solve the nonlinear aerosol dynamic equations by combining the discontinuous Galerkin formulations (or other formulations), which will be a very interesting next step work.

4 Error estimates of the semi-discrete wavelet scheme

In this section, we will analyze error estimates for the semi-discrete wavelet Galerkin scheme (3.17). Firstly, we will prove two lemmas concerning the behavior of $\mathcal{L}_1$, which are fundamental to our error estimates.

Lemma 4.1. *The operator $\mathcal{L}_1$ is semi-bounded with respect to the inner product on $L^2(\Omega)$. That is, there exists a constant $\alpha>0$ such that for $u\in H_E^1(\Omega)$*

$$\langle \mathcal{L}_1 u,u\rangle \leq \alpha\langle u,u\rangle. \tag{4.1}$$

Proof. From the definition of linear operator $\mathcal{L}_1$, we have

$$\begin{aligned}\langle \mathcal{L}_1 u,u\rangle &= -\Big\langle \big(G(x)u\big)_x,u\Big\rangle = -\int_0^1 \big(G(x)u\big)_x u dx\\ &= -\int_0^1 u d(G(x)u) = -G(1)u^2(1,t)+\int_0^1 G(x)uu'dx\\ &= -G(1)u^2(1,t)-\langle \mathcal{L}_1 u,u\rangle -\int_0^1 G'(x)u^2dx\\ &\leq -\langle \mathcal{L}_1 u,u\rangle -\int_0^1 G'(x)u^2dx.\end{aligned}$$

Consequently,

$$\langle \mathcal{L}_1 u,u\rangle \leq \alpha\int_0^1 u^2dx,$$

where $\alpha=\max_{x\in\Omega}|G'(x)|/2$. □

Lemma 4.2. *There exists a constant $\lambda>0$ such that*

$$\langle \mathcal{L}_1 u,v\rangle \leq \lambda\|u\|_1\|v\|,\quad \forall u\in H^1(\Omega),\quad \forall v\in L^2(\Omega). \tag{4.2}$$

Proof. By applying Hölder inequality and the bounds of $G'(x)$ and $G(x)$ in Ω, we have

$$\begin{aligned}\langle \mathcal{L}_1 u,v\rangle &= -\Big\langle \big(G(x)u\big)_x,v\Big\rangle = -\int_0^1 \big(G(x)u\big)_x v dx\\ &= -\int_0^1 \big(G'(x)uv+G(x)u'v\big)dx\\ &\leq \lambda\|u\|_1\|v\|.\end{aligned}$$

This completes the proof of this lemma. □

Then, we can analyze the errors of the semi-discrete scheme (3.17). We assume first that there exist positive constant M^* and positive integer J^* such that for $j \geq J^*$,

$$\|U\|_{L^\infty(0,T;L^2(\Omega))} \leq M^*. \tag{4.3}$$

The error bound is then obtained in terms of the norm of $\|u\|_{r+1}$ and $\|\partial u/\partial t\|_{r+1}$, where $0 \leq r \leq N-1$. Finally the assumption of boundedness of U is proved. Let w be the orthogonal projection of u into $V_j(\Omega)$. Denote

$$\eta = u - w, \quad \xi = w - U.$$

Then $u - U = \eta + \xi$.

Theorem 4.1. *Assume $u \in L^\infty(0,T;L^2(\Omega)) \bigcap H^{r+1}(\Omega)$ and $u_t \in H^{r+1}(\Omega)$ for $0 \leq r \leq N-1$. Let u be the solution of the problem (2.5); and let U, defined in (3.17), be the wavelet approximation of u, with the initial projection $P_j u_0$ of $u_0(x)$ onto $V_j(\Omega)$ with accuracy $\mathcal{O}(2^{-j(r+1)})$. Then there exists a constant C_4 such that*

$$\begin{aligned}\|u(t) - U(t)\| \leq & C_4 e^{(\alpha+R+K)t} 2^{-j(r+1)} \|u(0)\|_{r+1} + C_4 2^{-j(r+1)} \|u(t)\|_{r+1} \\ & + C_4 \frac{(e^{(\alpha+R+K)t} - 1)}{(\alpha+R+K)} 2^{-jr} \max_{0<s<t} \left\{ \|u(s)\|_{r+1} + \|\partial_t u(s)\|_{r+1} \right\}, \end{aligned} \tag{4.4}$$

where $K = 3\beta_0(M+M^*)/2$.

Proof. Subtracting (3.17) from (3.15) yields

$$\begin{aligned}\langle \xi_t, v \rangle = & -\langle \eta_t, v \rangle - \langle R(x)\xi, v \rangle - \langle R(x)\eta, v \rangle + \langle \mathcal{L}_1 \xi, v \rangle + \langle \mathcal{L}_1 \eta, v \rangle \\ & + \langle \mathcal{L}_2(u) - \mathcal{L}_2(U), v \rangle - \langle \mathcal{L}_3(u) - \mathcal{L}_3(U), v \rangle. \end{aligned} \tag{4.5}$$

Setting $v = \xi$ and applying Lemmas 4.1 and 4.2 and the estimates for the removal term give

$$\begin{aligned}\|\xi\| \frac{d}{dt} \|\xi\| \leq & \|\xi\| \|\eta_t\| + R\|\xi\|^2 + R\|\xi\| \|\eta\| + \alpha \|\xi\|^2 + \lambda \|\xi\| \|\eta\|_1 \\ & + \langle \mathcal{L}_2(u) - \mathcal{L}_2(U), \xi \rangle - \langle \mathcal{L}_3(u) - \mathcal{L}_3(U), \xi \rangle. \end{aligned}$$

To estimate the term $\langle \mathcal{L}_2(u) - \mathcal{L}_2(U), \xi \rangle$, we rewrite it as follows

$$\begin{aligned}\langle \mathcal{L}_2(u) - \mathcal{L}_2(U), \xi \rangle = & \frac{1}{2} \int_0^1 \left(\int_0^x \Big(\beta(x-y,y) u(x-y,t) u(y,t) \right. \\ & \left. - \beta(x-y,y) U(x-y,t) U(y,t) \Big) dy \right) \xi(x) dx \\ = & \frac{1}{2} \int_0^1 \left(\int_0^x \Big(\beta(x-y,y)(u(x-y,t) - U(x-y,t)) u(y,t) \right. \\ & \left. + \beta(x-y,y)(u(y,t) - U(y,t)) U(x-y,t) \Big) dy \right) \xi(x) dx. \end{aligned}$$

Applying Hölder inequality and combining the fact $\beta(x,y)\leq\beta_0$, it follows that

$$\begin{aligned}&\langle\mathcal{L}_2(u)-\mathcal{L}_2(U),\xi\rangle\\ &\leq\frac{\beta_0}{2}\int_0^1\left(\int_0^x(u(x-y,t)-U(x-y,t))^2dy\right)^{1/2}\left(\int_0^x u^2(y,t)dy\right)^{1/2}\xi(x)dx\\ &\quad+\frac{\beta_0}{2}\int_0^1\left(\int_0^x(u(y,t)-U(y,t))^2dy\right)^{1/2}\left(\int_0^x U^2(x-y,t)dy\right)^{1/2}\xi(x)dx.\end{aligned}$$

For the term $\int_0^x(u(x-y,t)-U(x-y,t))^2dy$ above, using the variable transformation $z=x-y$ gives

$$\begin{aligned}&\int_0^x(u(x-y,t)-U(x-y,t))^2dy\\ &=\int_0^x(u(z,t)-U(z,t))^2dz\leq\int_0^1(u(z,t)-U(z,t))^2dz.\end{aligned}\tag{4.6}$$

Combining (4.6), (4.3) and the fact $\|u\|_{L^\infty(0,T;L^2(\Omega))}\leq M$, we have the estimate

$$\langle\mathcal{L}_2(u)-\mathcal{L}_2(U),\xi\rangle\leq\frac{\beta_0}{2}(M+M^*)(\|\xi\|+\|\eta\|)\|\xi\|.$$

An estimate for $\langle\mathcal{L}_3(u)-\mathcal{L}_3(U),\xi\rangle$ can be derived in a similar way, which leads to the inequality

$$\langle\mathcal{L}_3(u)-\mathcal{L}_3(U),\xi\rangle\leq\beta_0(M+M^*)(\|\xi\|+\|\eta\|)\|\xi\|.$$

Thus

$$\begin{aligned}\|\xi\|\frac{d}{dt}\|\xi\|\leq&\|\xi\|\|\eta_t\|+R\|\xi\|^2+R\|\xi\|\|\eta\|\\ &+\alpha\|\xi\|^2+\lambda\|\xi\|\|\eta\|_1+K\|\xi\|^2+K\|\xi\|\|\eta\|,\end{aligned}$$

and we further have

$$\frac{d}{dt}\|\xi\|\leq(\alpha+R+K)\|\xi\|+(\|\eta_t\|+\lambda\|\eta\|_1+R\|\eta\|+K\|\eta\|).$$

An application of Gronwall's inequality to the above inequality yields

$$\|\xi(t)\|\leq e^{\alpha+R+K}\|\xi(0)\|+\int_0^t e^{(\alpha+R+K)(t-s)}(\lambda\|\eta\|_1+R\|\eta\|+K\|\eta\|+\|\partial_t\eta\|)ds.$$

Combining the fact that $\|\xi(0)\|\leq\|u(0)-U(0)\|+\|\eta(0)\|$, we obtain the result under the assumption (4.3).

Next we show (4.3) to complete the proof. Let $\|u\|_{L^\infty(0,T;L^2(\Omega)}\leq M$. Without loss of generality, we assume that $M^*>3M$. It follows from Approximation Property (3.10) that

$$\|U(0)\|\leq(1+C_1 2^{-j(r+1)})\|u(0)\|.\tag{4.7}$$

It follows from $\|u\|_{L^\infty(0,T;L^2(\Omega))} \leq M$ that

$$\|U(0)\| \leq 2M, \tag{4.8}$$

for sufficiently large j.

If the condition (4.3) was false, from the continuity of $\|U(t)\|$ in t and (4.8) there would be a $t_0 > 0$ independent of j such that $t_0 < T$ and

$$\|U(t)\| \leq M^*, \quad t \in [0,t_0), \tag{4.9}$$
$$\|U(t)\| > M^*, \quad t \in [t_0,T], \tag{4.10}$$

for sufficiently large j. From the result of error estimate (4.4),

$$\|U(t_0)\| < 2M < M^*, \tag{4.11}$$

for sufficiently large j, which is a contradiction of (4.10). Thus the proof is complete. □

5 Global existence of the semi-discrete wavelet approximation

In this part, we shall prove global existence and uniqueness of the nonlinear finite element approximation U of u in the domain of existence of u, by employing Schauder's fixed point theorem. For all $v \in V_j(\Omega)$,

$$\begin{aligned}\langle \partial_t \xi, v\rangle = &-\langle \partial_t \eta, v\rangle - \langle R(x)\xi, v\rangle - \langle R(x)\eta, v\rangle + \langle \mathcal{L}_1 \xi, v\rangle + \langle \mathcal{L}_1 \eta, v\rangle \\ &+ \langle \mathcal{L}_2(u) - \mathcal{L}_2(U), v\rangle - \langle \mathcal{L}_3(u) - \mathcal{L}_3(U), v\rangle,\end{aligned} \tag{5.1}$$

where $e = u - U = u - w + w - U = \xi + \eta$. This system is a nonlinear system in ξ. We will first linearize the system, and then apply Schauder's fixed point theorem. Replacing $U = u - e$ in (5.1) and substituting e by $E(x,t)$, where $E(x,t) \in L^2(0,T;H_E^1(\Omega))$, we obtain a linearized formulation form given by

$$\begin{aligned}\langle \partial_t \xi, v\rangle = &-\langle \partial_t \eta, v\rangle - \langle R(x)\xi, v\rangle - \langle R(x)\eta, v\rangle + \langle \mathcal{L}_1 \xi, v\rangle + \langle \mathcal{L}_1 \eta, v\rangle \\ &+ \langle \mathcal{L}_2(u) - \mathcal{L}_2(u-E), v\rangle - \langle \mathcal{L}_3(u) - \mathcal{L}_3(u-E), v\rangle.\end{aligned} \tag{5.2}$$

This is a linear ordinary differential equation of ξ. Therefore, for any $E = E(x,t)$, there exists a unique solution $\xi \in V_j(\Omega)$ of (5.2) in the interval $[0,T]$. Thus, Eq. (5.2) defines an operator B from $H_E^1(\Omega)$ to $V_j(\Omega)$ such that $\xi = B\{E\}$ for each $E \in H_E^1(\Omega)$. Since $e = \eta + \xi$, we define the operator $D : H_E^1(\Omega) \to H_E^1(\Omega)$ by $D\{E\} = \eta + B\{E\}$. We only need to show that the operator D has a fixed point E in $H_E^1(\Omega)$ in order to prove the existence of a solution $U(t) \in V_j(\Omega)$ to problem (3.17).

Theorem 5.1. *Let u be the exact solution to problem (2.1). Then, for $0 < \epsilon \leq 1$ and for sufficient large j, there exists a unique solution $U \in L^\infty(0,T;V_j(\Omega))$ to problem (3.17) such that*

$$\|u(t) - U(t)\| \leq \epsilon, \tag{5.3}$$

for $t \in (0,T]$.

Proof. Choose $v=\xi$ in (5.2) and apply Hölder inequality and boundedness of u and U to obtain

$$\frac{1}{2}\frac{d}{dt}\|\xi\|^2 \leq \alpha\|\xi\|^2+\alpha\|\eta\|_1\|\xi\|+R\|\xi\|^2+R\|\eta\|\|\xi\|+\|\partial_t\eta\|\|\xi\|+K\|E\|\|\xi\|.$$

Consequently,

$$\frac{d}{dt}\|\xi\| \leq (\alpha+R)\|\xi\|+(\alpha\|\eta\|_1+R\|\eta\|+\|\partial_t\eta\|+K\|E\|). \tag{5.4}$$

Applying Gronwall's inequality to (5.4) gives

$$\begin{aligned}&\|\xi\|_{L^\infty(0,T;L^2(\Omega))}\\ \leq& C_6\Big(\|\xi(0)\|+\|\eta\|_{L^\infty(0,T;H^1(\Omega))}+\|\partial_t\eta\|_{L^\infty(0,T;L^2(\Omega))}+\|E\|_{L^\infty(0,T;H^1(\Omega))}\Big),\end{aligned} \tag{5.5}$$

where C_6 is a constant independent of j and E. Combining (5.5), Approximation Property (3.10) and Inverse Property (3.11) yields

$$2^{-j}\|\xi\|_{L^\infty(0,T;H^1(\Omega))} \leq C_7 2^{-jr} \tag{5.6}$$

with $C_7>0$ independent of j but depending on E.

Then from (5.6), Approximation Property (3.10) and the definition of D, it follows, on noting $r\leq 2$, that for $j>1$ and some constant C_8

$$\|D\{E\}\|_{L^\infty(0,T;H^1(\Omega))} \leq C_8 2^{-j(r-1)}. \tag{5.7}$$

Thus, there exists an J^* such that for all $j\geq J^*$, $\|D\{E\}\|_{L^\infty(0,T;H^1(\Omega))}\leq\epsilon$. Then the operator D maps the sphere

$$B_\epsilon := \{E\in L^\infty(0,T;H^1(\Omega)) : \|E\|_{L^\infty(0,T;H^1(\Omega))}\leq\epsilon\}, \quad (0<\epsilon\leq 1) \tag{5.8}$$

into itself. Also, D is a continuous and compact operator. Hence, by Schauder's fixed point theorem, there exists an E in B_ϵ such that $D\{E\}=\{E\}$. The existence of the solution is thus established. □

For uniqueness, let us assume that U_1 and U_2 are two solutions to scheme (3.17) with the same initial value projection. Then,

$$\langle\partial_t U_1,v\rangle = \langle\mathcal{L}_1 U_1,v\rangle-\langle R(x)U_1,v\rangle+\langle\mathcal{L}_2(U_1),v\rangle-\langle\mathcal{L}_3(U_1),v\rangle, \tag{5.9}$$

and

$$\langle\partial_t U_2,v\rangle = \langle\mathcal{L}_1 U_2,v\rangle-\langle R(x)U_2,v\rangle+\langle\mathcal{L}_2(U_2),v\rangle-\langle\mathcal{L}_3(U_2),v\rangle. \tag{5.10}$$

Subtracting (5.10) from (5.9), we get

$$\begin{aligned}\langle \partial_t(U_1-U_2),v\rangle =&\langle \mathcal{L}_1(U_1-U_2),v\rangle -\langle R(x)(U_1-U_2),v\rangle \\ &+\langle \mathcal{L}_2(U_1)-\mathcal{L}_2(U_2),v\rangle -\langle \mathcal{L}_3(U_1)-\mathcal{L}_3(U_2),v\rangle .\end{aligned} \tag{5.11}$$

Let $v=U_1-U_2$. Then it follows from (5.11) that

$$\|U_1-U_2\|\frac{d}{dt}\|U_1-U_2\|\leq(\alpha+R+K)\|U_1-U_2\|^2. \tag{5.12}$$

Integrating (5.12) from 0 to t with respect to time gives

$$\|U_1(t)-U_2(t)\|^2\leq\|U_1(0)-U_2(0)\|^2e^{2(\alpha+R+K)t}. \tag{5.13}$$

From the assumptions on the initial values $U_1(0)=U_2(0)$, we have $U_1(t)-U_2(t)=0$ for all t in $[0,T]$.

6 Error estimates of the fully-discrete wavelet scheme

The fully-discrete wavelet Galerkin scheme (3.18) can be easily shown to have unique solution. In this section, we will analyze the error estimates to the fully-discrete wavelet scheme. Let u be the exact solution of problem (2.5) and U^l, $0\leq l\leq L$, be the solution of problem (3.18). We have the following error estimate result.

Theorem 6.1. *Assume* $0<(\alpha+R)\Delta t<1$, $u_{ttt}\in L^\infty(0,T;L^\infty(\Omega))$, $u\in L^\infty(0,T;H^{r+1}(\Omega))$, $\|u\|_{L^\infty(0,T;L^2(\Omega))}\leq M$ *and* $u_t\in L^\infty(0,T;H^{r+1}(\Omega))$. *Then there are positive constants* C_5 *and* δ, *where* $\delta=\frac{\alpha+R+K}{1-(\alpha+R)\Delta t}<2(\alpha+R+K)$ *when* Δt *is small enough, such that*

$$\begin{aligned}\|u^l-U^l\|\leq&C_5\Big\{2^{-j(r+1)}\Big(\|u_0\|_{r+1}+\|\partial_t u\|_{L^\infty(H^{r+1})}\Big)\\ &+2^{-jr}\|u\|_{L^\infty(H^{r+1})}+\Delta t\max_{t,x}|u_{ttt}|\Big\}\end{aligned} \tag{6.1}$$

holds for $l=1,2,\cdots,L$.

Proof. Let $u^l(x)$ denote $u(x,l\Delta t)$. Then u^l satisfies

$$\begin{aligned}\left\langle\frac{u^{l+1}-u^l}{\Delta t},v\right\rangle=&\langle\mathcal{L}_1u^{l+1},v\rangle-\left\langle R(x)u^{l+1},v\right\rangle\\ &+\left\langle\mathcal{L}_2(u^l),v\right\rangle-\left\langle\mathcal{L}_3(u^l),v\right\rangle+\left\langle r^l,v\right\rangle,\end{aligned} \tag{6.2}$$

where $r^l=(u^{l+1}-u^l)/\Delta t-(\partial/\partial t)(u^l)$. Subtracting (3.18) from (6.2), we obtain

$$\begin{aligned}\left\langle\frac{\xi^{l+1}-\xi^l}{\Delta t},v\right\rangle=&-\left\langle\frac{\eta^{l+1}-\eta^l}{\Delta t},v\right\rangle-\langle R(x)\xi^{l+1},v\rangle-\langle R(x)\eta^{l+1},v\rangle+\langle r^l,v\rangle\\ &+\langle\mathcal{L}_1\xi^{l+1},v\rangle+\langle\mathcal{L}_1\eta^{l+1},v\rangle+\langle\mathcal{L}_2(u^l)-\mathcal{L}_2(U^l),v\rangle-\langle\mathcal{L}_3(u^l)-\mathcal{L}_3(U^l),v\rangle.\end{aligned}$$

Choosing $v=\xi^{l+1}$ and taking the similar process of Theorem 4.2, we have the following estimate

$$(1-\alpha\Delta t-R\Delta t)\|\xi^{l+1}\|\leq(1+K\Delta t)\|\xi^{l}\|+\lambda\Delta t\|\eta^{l+1}\|_1 \\ +(1+\Delta tR)\|\eta^{l+1}\|+(1+K\Delta t)\|\eta^{l}\|+\Delta t\|r^{l}\|.$$

Applying Gronwall's inequality, there exists a constant C such that

$$\|\xi^{l}\|\leq Ce^{\delta t}\|\xi^{0}\|+Ce^{\delta t}\max_{0<s<t,0\leq l\leq T/\Delta t}\left\{\left\|\frac{\eta(s+\Delta t)-\eta(s)}{\Delta t}\right\|+\|\eta(s)\|_1+\|r^{l}\|\right\}$$

and $\|(\eta^{l+1}-\eta^{l})/\Delta t\|\leq C\|\partial\eta/\partial t\|$, and the estimate $\|r^{l}\|\leq C\Delta t\max|u_{ttt}|$ follows from Taylor's expansion. Combining Approximation Property (3.10) and the triangle inequality from $u^{l}-U^{l}=\xi^{l}+\eta^{l}$, we can easily obtain the error estimates for the finite element approximation U^{l} to the original solution u^{l}. □

7 Numerical experiments

In this part, we will take numerical experiments to study the aerosol dynamics by the wavelet Galerkin method. For the first example with analytical solution, we compare the wavelet Galerkin method with the finite difference method to show the accuracy and effectiveness of our method. A general example of aerosol dynamics will be given in Example 7.2 which describes the joint effect of condensation and coagulation processes in continuum size regime with an initial log-normal distribution. In Example 7.3, a real aerosol deposition process is simulated with a three-modes initial distribution.

Example 7.1. For the first experiment we consider a test problem (see [31]). This problem has analytical solution which is normally used to test the numerical accuracy of numerical methods. We consider a constant coagulation rate β_0 and linear growth rate $G(x)=\sigma_0 x$. The initial number distribution is exponential

$$u(x,0)=(N_0/X_m)e^{-x/X_m},$$

where N_0 is the initial number of aerosol particles and X_m is the initial mean volume. The distribution is truncated to the interval with lower and upper limits of volume size $X_{\min}=0\mu m^3$ and $X_{\max}=\pi/6\mu m^3$. Take $\sigma_0=0.05/hour$, $N_0=10^4 particles/cm^3$ and $X_m=0.03\mu m^3$.

The analytical solution is given as

$$u^{A}(x,t)=\frac{4N_0}{X_m(N_0\beta_0 t+2)^2}\exp\left(-\frac{2x\exp(\sigma_0 t)}{X_m(N_t\beta_0 t+2)}-\sigma_0 t\right),\quad (x,t)\in\left(0,\frac{\pi}{6}\right)\times(0,T]. \tag{7.1}$$

In the computation, we choose 2^J wavelet bases for the wavelet Galerkin method and take the uniform grid for the finite difference method with $\Delta x=(X_{\max}-X_{\min})/2^J$.

Three tests are performed for problems of (i) condensation-only (β_0=0), (ii) coagulation-only (σ_0=0), and (iii) joint condensation-coagulation. Let $u_i(T)$ be the numerical solution at volume nodes $x_i=i\Delta x$ and $u^A(x_i,t_j)$ be the analytical solution value. The error is measured in the root mean square (RMS) norm at the node points:

$$Err=\sqrt{\frac{1}{s}\sum_{i=1}^{s}\frac{[u_i(T)-u^A(x_i,T)]^2}{\max(u^A(x_i,T),Thr)^2}}, \tag{7.2}$$

where the threshold is $Thr=1000\ particles/cm^3\mu m^3$, and $s=1+2^J$ is the total number of volume nodes.

The numerical errors of wavelet Galerkin method and finite difference method at time $T=5h$ are shown in Table 1. With the same time step size $\Delta t=1/100h$ and different J, numerical solutions of the wavelet Galerkin method even with few wavelet bases approximate exact solutions better.

Table 1: Numerical errors in (RMS) norm.

Level number	Condensation only		Coagulation only	Condensation	Coagulation
	WG	FD	WG	WG	FD
$J=4$	0.0781	0.3006	0.1511	0.2028	0.6448
$J=5$	0.0411	0.1088	0.0556	0.0712	0.1513
$J=6$	0.0403	0.0486	0.0441	0.0491	0.0561

The numerical analytical volume distributions, defined as volume times number distributions, at different times $t=5h$, $t=10h$ and $t=15h$ for condensation only process are shown in Fig. 1. We can see that the numerical solutions are in excellent agreement with the analytical solution at different times. The total volume of aerosol particles increases as a result of vapors condensing. The principle of some certain atmospherical aerosol volume density is that the density curve is in slanting distribution, which means on the side of smaller size, volume density decreases rapidly, while on the side of larger size, volume density decreases slowly. When

$$x_c=\frac{6X_m\sigma_0 T}{\pi(1-e^{-\sigma_0 T})},$$

the volume density reaches its maximum point. We can also see the principle from the graph, the size distribution decreases strongly on the side of the smaller side; after x passes the critical point x_c, the size distribution decreases slowly. Our simulation results explain this principle well.

Example 7.2. In this example, we simulate the joint effect of condensation and coagulation processes in continuum size regime. When the vapor pressure increases and air mean free path decreases, then the condensation and coagulation will be considered to

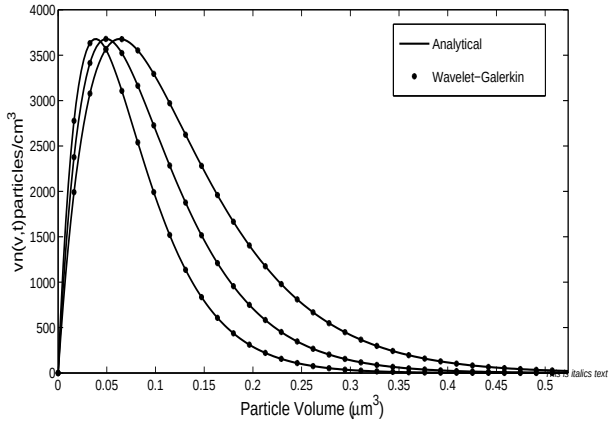

Figure 1: The volume distributions for condensation-only process by the wavelet Galerkin method and analytical solution distribution at different times $t=5h$, $t=10h$ and $t=15h$ with $J=5$ and $\Delta t=1/20h$.

be in continuum size regime [19, 23]. In this case, the condensation growth rate has the form

$$G_C(x)=B_3x^{1/3}(S-1), \tag{7.3}$$

where $B_3=(48\pi^2)^{1/3}Dv_1n_s$, and $D=\lambda(8k_BTe/\pi m_1)^{1/2}/3$. Take the saturation ratio $S=1.521$, the standard temperature $Te=298K$, the monomer mass $m_1=5.33\times10^{-26}kg$, the monomer volume $v_1=5.33\times10^{-5}\mu m^3$, the Boltzmann's constant $k_B=1.38\times10^{-23}JK^{-1}$, and $n_s=2.43\times10^{-4}molecules/\mu m^3$, the mean free path $\lambda=6.5\times10^{-2}\mu m$, then $B_3(S-1)=1\times10^2\mu m/s$. Let the temperature $Te=298K$ and the dynamic viscosity of air $\mu_{air}=1.82\times10^1kg/ms$. The coagulation kernel is defined in (2.4).

The initial distribution is chosen to be the sum of two log-normal distributions

$$n_0(x)=\sum_{i=1}^{2}\frac{N_i}{3\sqrt{2\pi}\ln\sigma_i}\exp\left(-\frac{\ln^2(x/x_{gi})}{18\ln^2\sigma_i}\right)\frac{1}{x}$$

on the volume domain $\Omega=[1\times10^2\mu m^3,1\times10^{4.5}\mu m^3]$ with $N_1=5\times10^4particles/\mu m^3$, $N_2=2\times10^4particles/\mu m^3$, $x_{g1}=1\times10^{2.7}\mu m^3$, $x_{g2}=1\times10^{3.5}\mu m^3$, $\sigma_1=1.13$ and $\sigma_2=1.2$.

In this example, we take logarithmic scale for the sizes of studied aerosol particles spans orders of magnitude and it can describe the aerosol region more effectively. Take log transformation for aerosol volume with the time step size $\Delta t=0.1s$ and $J=6$. The numerical number distributions $3xn(x,t)$ for the condensation process in the continuum size regime at time $T=0s$, $T=25s$, $T=50s$ and $T=75s$ are shown in Fig. 2. The horizontal coordinate indicates the $\ln(r)$, where r is the diameter of aerosol particles with the unit of μm. Moreover, the vertical coordinate refers to the values of aerosol number distribution $3xn(x,t)$. Actually, $3xn(x,t)$ equals to $dN_{tol}/d\ln(r)$. Consequently, the number distribution is

$$\frac{dN_{tol}}{d\ln(r)}=r\frac{dN_{tol}}{dr}=r\frac{dN_{tol}}{dx}\frac{dx}{dr}=4\pi r^3\frac{dN_{tol}}{dx}=3xn(x,t),$$

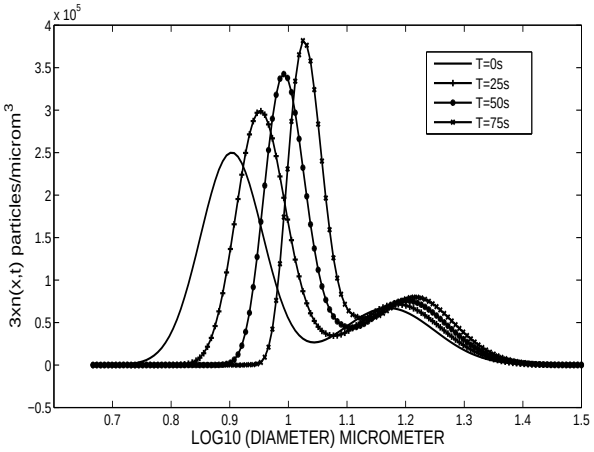

Figure 2: The numerical number distributions of $3vn(v,t)$ of the joint condensation and coagulation process in the continuum size regime at $T=0s$, $T=25s$, $T=50s$ and $T=75s$.

where N_{tol} is the total number concentration of aerosol particles (see [5, 31]). With the increasing of time, the total volumes of aerosol particles grow due to the condensation process of vapors condensing on aerosol particles. While the number distribution of the aerosol particles in the intermediate part of the two lognormal peaks decreases because the decrease of number distribution due to coagulation process is greater than the increase due to condensation growth. The coagulation process of smaller particles results in the increase of the number concentration of larger particles.

Table 2: Log-normal parameters for continental aerosols.

	nucleation mode	accumulation mode	coarse mode
$N(cm^{-3})$	7.7×10^4	1.3×10^4	4.2
$r_g(\mu m)$	0.013	0.069	0.97
σ_g	1.7	2.03	2.15

Example 7.3. In this example, we consider the aerosol dry deposition process. The initial distribution is the sum of three modes: the nucleation mode, accumulation mode and coarse mode ([35, 36]). Each mode has a lognormal distribution form:

$$n(r,0)=\frac{N}{\sqrt{2\pi}\ln\sigma_g r}\exp(-\frac{\ln^2(r/r_g)}{2\ln^2\sigma_g}).$$

Table 2 lists some typical values of the total number concentration N, geometric mean diameter r_g and the geometric standard deviation σ_g for continental aerosols. We will choose these parameters as the initial distribution of our simulation of dry deposition process. The concerned domain is $\Omega=[1\times10^{-9}m,1\times10^{-4}m]$.

We take the logarithmic scale for diameter direction, then change the range of $\ln r$ into x in [0,1]. Take the uniform time grids with the step size Δt on the t-direction. Fix $J=5$, we choose 2^J wavelet base functions to approximate the number density function on volume direction, $\Delta x = 1/2^{J+1} \approx 0.0156$, and $\Delta t = 0.1$.

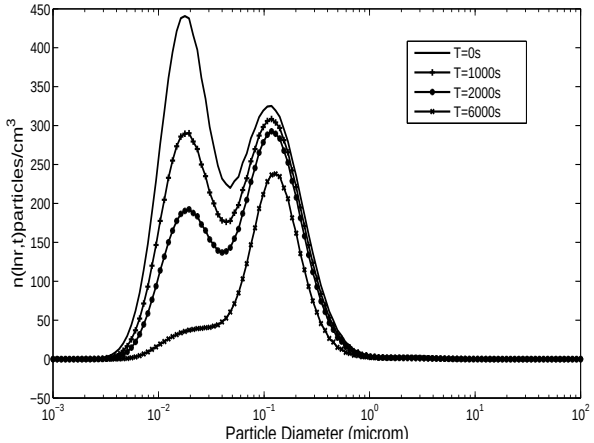

Figure 3: The volume distributions for dry deposition process with the wind speed $u=5ms^{-1}$ at $T=0s$, $T=1000s$, $T=2000s$ and $T=6000s$.

The numerical solutions for the dry deposition process of aerosol dynamics at different times $T=0s$, $T=100s$, $T=2000s$ and $T=6000s$ are shown in Fig. 3. The horizontal coordinate indicates the aerosol particle diameter and the vertical coordinate refers to the volume distribution of $\ln r$, which is $dv/d\ln(r)$. The reason to choose volume distribution not number distribution is to better show the distribution of three modes. The coarse mode is not shown in this graph due to comparatively very small total number concentration. Dry deposition velocity V_d decreases exponentially with the increasing of particle diameter in the size range $[1\times10^{-9},1\times10^{-6}]$. It is seen that volume distribution $dv/d\ln(r)$ has lower values with the increasing of time for all particle size ranges. Values of nucleation mode decrease dramatically, while values of accumulation mode become lower slowly since dry deposition velocity V_d of nucleation mode is much larger than that of accumulation mode. At $T=6000s$, the volume distribution is totally different from the original volume distribution, values of nucleation mode are smaller than those of accumulation mode.

8 Conclusion

We studied mathematical modeling of nonlinear aerosol dynamic equations by the wavelet Galerkin methods. We obtained the theoretical analysis of the wavelet methods for the problem. The existence and uniqueness for the continuous time wavelet Galerkin scheme were proved using the Schauder's fixed point theorem. We further obtained error esti-

mates for both the continuous time and discrete time wavelet Galerkin schemes. Numerical solutions of the wavelet method showed its superiority compared with the finite difference method even with few wavelet bases. For the aerosol distribution examples, the wavelet method obtained efficient numerical simulating results. Our future work will focus on the development and analysis of adaptive wavelet methods for the aerosol dynamic equations.

Acknowledgments

The authors thank the referee for the valuable suggestions which have helped to improve the paper greatly. This work was supported partly by National Engineering and Science Research Council of Canada and by Canadian Foundation for Climate and Atmospheric Sciences.

References

[1] A. Avudainayagam and C. Vani, Wavelet-Galerkin solutions of quasilinear hyperbolic conservation equations, Comm. Numer. Methods Engrg., 15 (1999), 589-601.
[2] I. J. Ackermann, H. Hass, M. Memmesheimer, A. Ebel, F. S. Binkowski and F. Shankar, Modal aerosol dynamics model for Europe: development and first applications, Atmos. Environ., 32 (1998), 2981-2999.
[3] S. Bertoluzza and G. Naldi, A wavelet collocation method for the numerical solution of partial differential equations, Appl. Comput. Harmon. Anal., 3(1996), 1-9.
[4] G. Beylkin, R. Coifman and V. Rokhlin, Fast wavelet transforms and numerical algorithms, I. Comm. Pure Appl. Math., 44 (1991), 141-183.
[5] J. R. Brock and J. Oates, Moment simulation of aerosol evaporation, J. Aerosol. Sci., 18 (1987), 59-64.
[6] J. R. Cannon and D. M. Elwood, A system involving a nonlinear first-order partial differential equation coupled with a nonlinear Volterra integral equation, SIAM J. Appl. Math., 50 (1990), 1001-1013.
[7] M. Q. Chen, C. Hwang and Y. P. Shih, The computation of wavelet-Galerkin approximation on a bounded interval, Int. J. Numer. Meth. Eng., 39 (1996), 2921-2944.
[8] X. F. Chen, S. J. Yang, J. X. Ma and Z. J. He, The construction of wavelet finite element and its application, Finite. Elem. Anal. Des., 40 (2004), 541-554.
[9] Z. Chen, C. A. Micchelli and Y. Xu, A construction of interpolating wavelets on invariant sets, Math. Comp., 68 (1999), 1569-1587.
[10] Z. Chen, C. A. Micchelli and Y. Xu, A multilevel method for solving operator equations, J. Math. Anal. Appl., 262 (2001), 688-699.
[11] A. Cohen, Numerical analysis of wavelet methods, Amsterdam ; Boston : Elsevier, 2003.
[12] A. Cohen, I. Daubechies and P. Vial, Wavelets on the interval and fast wavelet transforms, Appl. Comput. Harmon. Anal., 1 (1993), 54-81.
[13] A. Cohen and R. Masson, Wavelet methods for second-order elliptic problems, preconditioning, and adaptivitiy, SIAM. J. Sci. Comput., 21 (1999), 1006-1026.
[14] W. Dahmen, S. Prossdorf and R. Schneider, Multiscale methods for pseudodifferential equations, Z. Angew. Math. Mech., 76 (1996), suppl. 1, 7-10.

[15] W. Dahmen, R. Schneider and Y. Xu, Nonlinear functionals of wavelet expansions-adaptive reconstruction and fast evaluation, Numer. Math., 86 (2000), 49-101.
[16] I. Daubechies, Ten Lectures on Wavelets, Philadelphia, PA, USA, SIAM, 1992.
[17] E. Debry, B. Sportisse and B. Jourdain, A stochastic approach for the numerical simulation of the general dynamics equation for aerosols, J. Comput. Phys., 184 (2003), 649-669.
[18] J. L. Diaz Calle, P. R. B. Devloo, S. M. Gomes, Wavelets and adaptive grids for the discontinuous Galerkin method, Numer. Alg., 39 (2005), 143-154.
[19] A. Elgarayhi and A. Elhanbaly, General solution of the aerosol dynamic equation: growth and diffusion processes, J. Quant. Spectrosc. Ra., 86 (2004), 371-378.
[20] S. K. Friedlander, Smoke, Dust and Haze, John Wiley and Sons, New York, 1977.
[21] F. Gelbard, Y. Tambour and J. H. Seinfeld, Sectional representations for simulating aerosol dynamics, J. Colloid. Interf. Sci., 76 (1980), 541-556.
[22] M. Z. Jacobson, Fundamentals of Atmospheric Modelling, Cambridge University Press, Cambridge, 1999.
[23] L. Jameson, On the wavelet based differentiation matrix, J. Sci. Comput., 8 (1993), 267-305.
[24] Y. Liu and I. T. Cameron, A new wavelet-based method for the solution of the population balance equation, Chem. Eng. Sci., 56 (2001), 5283-5294.
[25] S. Mallat, Multiresolution approximation and wavelets, Trans. Amer. Math. Soc., 315 (1989), 69-88.
[26] Y. Meyer, Ondelettes due I'intervalle, Rev. Math. Iberoamericana., 7 (1992), 115-133.
[27] C. A. Micchelli and Y. Xu, Using the matrix refinement equation for the construction of wavelets on invariant sets, Appl. Comp. Harmonic. Anal., 1 (1994), 391-401.
[28] C. A. Micchelli and Y. Xu, Reconstruction and decomposition algorithms for biorthogonal wavelets, Multidim. Syst. Sign. P., 8 (1997), 31-69.
[29] C. A. Micchelli, Y. Xu, and Y. Zhao, Wavelet Galerkin methods for second-kind integral equations, J. Comput. Appl. Math., 86 (1997), 251-270.
[30] O. Roussel, K. Schneider, A. Tsigulin and H. Bockhorn, A conservation fully adaptive multiresolution algorithm for parabolic PDEs, J. Comput. Phys., 188 (2003), 493-523.
[31] A. Sandu and C. Borden, A framework for the numerical treatment of aerosol dynamics, Appl. Numer. Math., 45 (2003), 475-497.
[32] Y. Seo and J. R. Brock, Distribution for moment simulation of aerosol evaporation, J. Aerosol. Sci., 4 (1990), 511-514.
[33] T. Von. Petersdorff and C. Schwab, Wavelet discretizations of parabolic integrodifferential equations, SIAM J. Numer. Anal., 41 (2003), 159-180.
[34] J. Walden, Orthonormal compactly supported wavelets for solving hyperbolic PDEs, Technical Report 170, Uppsala University, Department of Scientific Computing, Sweden, 1995.
[35] E. R. Whitby and P. H. McMurry, Modal aerosol dynamics modelling, Aerosol. Sci. Tech., 27 (1997), 673-688.
[36] K. T. Whitby, The physical characteristics of sulfur aerosols, Atmos. Environ., 12 (1978), 135-159.
[37] J. Xu and W. Shann, Galerkin-wavelet methods for two-point boundary value problems, Numer. Math., 63 (1992), 123-144.